Growth of 4-*N*,*N*-Dimethylamino-4′-*N*′-methyl-stilbazolium Tosylate (DAST) Organic Single Crystals Controlled by Oleic Acid

Xin Wen [1], Xiangdong Xu [1],*, Huaxin Zhou [1], Lu Hu [1], Yangyang Jing [1], Jimmy Xu [2], Xiaomeng Cheng [1], Jia Shi [3], Xinfeng Liu [3], Ting Fan [4], Mingang Zhang [1] and Yu Gu [1]

[1] State Key Laboratory of Electronic Thin Films and Integrated Devices, School of Optoelectronic Science and Engineering, University of Electronic Science and Technology of China (UESTC), Chengdu 610054, China; 201721050123@std.uestc.edu.cn (X.W.); 201622050439@std.uestc.edu.cn (H.Z.); 201721050108@std.uestc.edu.cn (L.H.); 201722050408@std.uestc.edu.cn (Y.J.); 201711050110@std.uestc.edu.cn (X.C.); 201721050131@std.uestc.edu.cn (M.Z.); 201611050111@std.uestc.edu.cn (Y.G.)

[2] School of Engineering, Brown University, Providence, RI 02912, USA; jimmy_xu@brown.edu

[3] CAS Key Laboratory of Standardization and Measurement for Nanotechnology, CAS Center for Excellence in Nanoscience, National Center for Nanoscience and Technology, Beijing 100190, China; shijia@nanoctr.cn (J.S.); liuxf@nanoctr.cn (X.L.)

[4] Chengdu Institute of Organic Chemistry, Chinese Academy of Sciences, Chengdu 610014, China; fanting@cioc.ac.cn

* Correspondence: xdxu@uestc.edu.cn; Tel.: +86-028-83208959

Abstract: 4-*N*,*N*-dimethylamino-4′-*N*′-methyl-stilbazolium tosylate (DAST) organic single crystals controlled by (Z)-Octadec-9-enoic acid (oleic acid, OA) was grown by a slow-cooling method. The as-grown DAST single crystals were systematically characterized by FTIR, X-ray diffraction, second harmonic generation, and UV-vis spectroscopy. Results indicate that addition of OA into the DAST solutions leads to the controlled growth of DAST single crystals and consequently, the crystal quality and optical properties can be modified. Particularly, the DAST crystals grown under the control of OA exhibit larger sizes, higher crystallinities, and better optical qualities with higher optical band gaps and lower defect density, compared with those grown in the absence of OA. These results are helpful for better understanding the controlled growth of DAST organic single crystals and modifying their properties for practical applications.

1. Introduction

4-*N*,*N*-dimethylamino-4′-*N*′-methyl-stilbazolium tosylate (DAST) organic single crystals have attracted considerable attention, owing to their large nonlinear optical (NLO) susceptibility, high electro-optical (EO) coefficient, and low dielectric constant [1,2]. Wide applications of DAST crystals include optical frequency conversion and information processing, terahertz (THz) wave generation and detection, and light-matter coupling [3–6], etc. For the practical applications, DAST single crystals with a large size, high crystallinity, and low defect density are generally required, by which higher NLO and EO properties can be achieved [7,8]. Conversely, a high defect density will cause negative effects on the interactions between the anions and cations of DAST as well as the ordered arrangement of the DAST molecules, thus leading to the decrease of the second-order nonlinear optical coefficient of DAST, and observation of weakened NLO properties, such as second harmonic generation (SHG)

and optical rectification. Similarly, the refractive index of the DAST crystals representing the EO properties will also be negatively affected by the defects. Moreover, high defect density will induce higher drift current, thus reducing the breakdown voltage, and affecting the insulation performance of organic DAST. Therefore, DAST single crystals with a large size and low defect density is highly attractive for both academic research and the industry. Unfortunately, the growth of bulk DAST single crystals with a large size and high optical quality has remained a challenge [9,10]. In the past decades, many methods for the growth of desirable DAST single crystals have been reported. For example, Hameed and co-workers added sodium 4-methylbenzenesulfonate (NaTS) into the DAST solution, thus yielding large and NaTS-doped DAST crystals by a slow-cooling method [11,12]. In contrast, Hao et al. reported that an appropriate amount of 4-Methylbenzenesulfonic acid (PTSA) additives can improve the stability of the growth solution, where the crystal structure and functional groups of DAST remain unchanged [13]. Recently, Thomas and co-workers described a method by adding (Z)-Octadec-9-enoic acid (oleic acid, OA) into the DAST solution, thus producing the DAST crystals with less hygroscopicity by a solvent evaporation method [14]. However, this previous work mainly focused on the nucleation and morphology of the resulting DAST crystals [14]. The optical properties and quality of the as-grown DAST crystals still remain unclear to date.

In this work, DAST single crystals were grown with and without the control of the OA by a slow-cooling method. Particularly, we paid special attention to the effects of OA additives on the optical properties and quality of the as-grown DAST single crystals, which have been systematically investigated in this work by Fourier infrared spectroscopy (PE Spectrum 400, PerkinElmer Inco., Waltham, MA, USA), X-ray diffraction (XRD, X'Pert Pro MPD, Malvern Panalytical Ltd., Almelo, The Netherlands), UV-vis spectroscopy (UV-1700, SHIMADZU Co., Kyoto, Japan), and SHG measurements, respectively. The SHG measurements was carried out from a Ti:sapphire femtosecond pulse laser with 76 MHz pulse rate.

2. Experimental Details

All chemicals, used with analytical grade and without purification, were purchased from Cologne chemical Co., Ltd. (Chengdu, China). The process for the synthesis and purification of DAST has been described elsewhere [15]. Based on the as-synthesized DAST, the DAST single crystals were further grown with and without the control of OA by the slow-cooling method under the same conditions. For the growth without the OA control, an excess amount of DAST powders (8.5 mmol, 3.5 g) were dissolved in methanol (100 mL). In contrast, for the growth under the control of the OA, the saturated solution was prepared by dissolving an equimolar ratio of DAST (8.5 mmol, 3.5 g) and OA (8.5 mmol, 2.4 g) into the same volume (100 mL) of methanol. Both solutions were prepared and transferred to separate beakers, each with a Teflon plate, both of which were kept at 55 °C for two days to achieve the homogeneity. Then, the saturated solutions were cooled from 55 to 45 °C, where nucleation did not occur. Subsequently, the solutions were cooled down from 45 to 43 °C with a cooling rate of 0.5 °C/day. Tiny crystals were observed in the solution at 43 °C, and then the temperature was kept for one day. Furthermore, the solutions were cooled down from 43 to 39 °C with a cooling rate of 0.3 °C/day. Finally, the solution was cooled down from 39 to 27 °C with a cooling rate of 1 °C/day, by which DAST single crystals were yielded. The growths of DAST single crystals with and without the OA control were carried out under the same conditions for 30 days.

3. Results and Discussion

The molecular structures of DAST and the OA additive are shown schematically in Figure 1a,b, respectively. As a comparison, Figure 2 shows the photographs of the largest DAST single crystals grown with and without the OA control. One can see that without the OA control, a crystal with a size of $5.8 \times 5.5 \times 0.9$ mm^3 was yielded (Figure 2a), where the growth rates along the *a*- and *b*-axes are almost the same, but the growth rate along the *c*-axis is relatively slow. In contrast, the largest DAST crystal grown under the control of the OA over the same time has a relatively larger size of

$11 \times 8 \times 1.2$ mm^3, as shown in Figure 2b. It is worth noting that compared with the typical DAST crystal grown without the OA control (Figure 2a), the morphology of the DAST crystal grown under the control of the OA is of an irregular hexagonal shape rather than a square platelet, but both crystals have the same crystal plane of (001) as the largest area. We note that the morphologies of the DAST single crystals grown under the control of the OA by the slow-cooling method as in this work are similar with those previously grown by the solvent evaporation method [14]. For the growth of DAST crystal under the control of the OA, the (010) face of DAST emerges since the oxygen atoms are exposed to the solution and OA for the (010) face, thus causing the formation of hydrogen bonds between the hydroxyl group of OA and the oxygen of DAST anions [14]. Interestingly, the OA addition inhibits the complete growth of the (010) face of DAST [14], and consequently, the crystal with an irregular hexagonal shape is observed in this case. As a result, the growth rate along the *b*-axis was inhibited, thus leading to the growth rate being slower along the *b*-axis than that along the *a*-axis in the OA case. Moreover, Figure 2 reveals that both growth rates along the *a*- and *b*-axis are higher in the crystal grown under the control of the OA than those in the crystal grown without the OA control. It is worth noting that the sizes of both DAST single crystals grown with ($11 \times 8 \times 1.2$ mm^3) and without ($5.8 \times 5.5 \times 0.9$ mm^3) the control of the OA by the slow-cooling method as in this work are significantly larger than those ($6 \times 3 \times 1$ mm^3 and $3 \times 1.5 \times 0.5$ mm^3, respectively) previously grown by the solvent evaporation method [14].
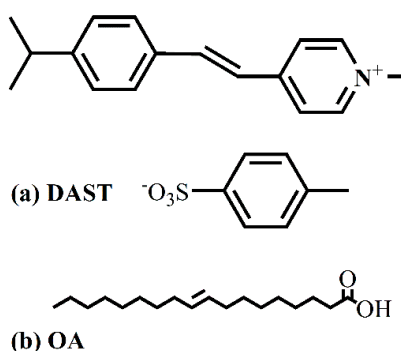

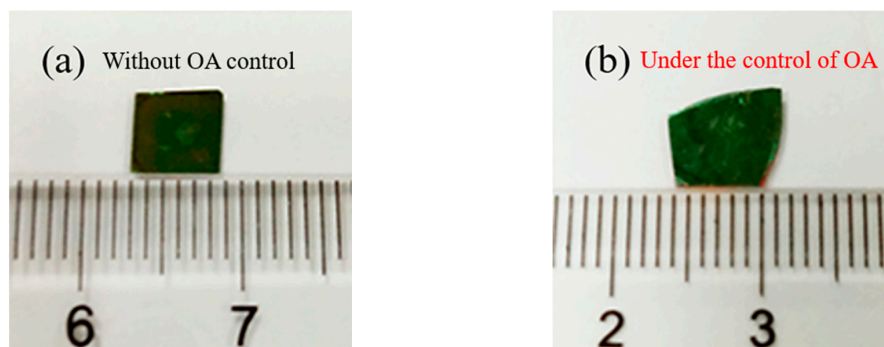**Figure 1.** Molecular structures of (**a**) DAST and (**b**) OA, respectively.

Figure 2. Photographs of the largest DAST single crystals grown (**a**) without the OA control ($5.8 \times 5.5 \times 0.9$ mm^3), and (**b**) under the control of the OA ($11 \times 8 \times 1.2$ mm^3).

The characterization of the products by mid-infrared (MIR) spectroscopy provides further chemical information. The typical MIR spectra in the wavenumber range of 4000–400 cm^{-1} for the DAST crystals grown with and without the OA control are shown in Figure 3. The characteristic MIR peaks in these spectra are assigned as: aromatic C-H stretching mode at 3033 cm^{-1}, C=C stretching mode of vibrations at 1642 cm^{-1}, aromatic ring vibrations at 1580 and 1527 cm^{-1}, CH$_3$ bending absorption mode and C-N stretching mode at 1373 cm^{-1}, SO$_3^-$ symmetric stretching vibration at 1171 cm^{-1}, 1,4-distribution in the aromatic ring at 820 cm^{-1}. The absorptions in the wavenumber range from 500

to 1000 cm^{-1} are attributed to the substituent group of the aromatic ring vibrations [16,17]. It is clear that the DAST crystal grown under the control of the OA exhibits similar IR features like that of the DAST crystal grown without the OA control (Figure 3), both of which are in accordance with those previously reported about DAST single crystals [18]. This indicates that both DAST crystals grown with and without the OA control have the same chemical structures. In other words, the OA additive has not been significantly incorporated into the as-grown DAST single crystals.
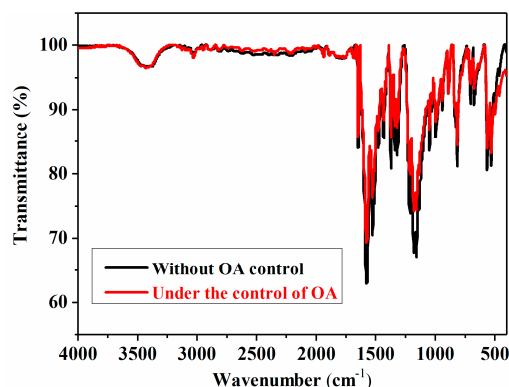
Figure 3. Typical MIR spectra of the DAST single crystals grown with and without the OA control.

The X-ray diffraction (XRD) spectra of the DAST crystals grown with and without the OA control are shown in Figure 4. Both major peaks were detected at 10°, 20°, 30°, and 40°, corresponding to the (002), (004), (006), and (008) planes of the DAST with the monoclinic space group Cc [11,14,15]. No additional peaks are observed in the range of 5–50°, verifying that OA neither changes the monoclinic crystal structure of the DAST nor induces polymorphism. Moreover, their narrow full widths at half maximum (FWHM) and strong intensities are indicative of excellent crystallinity [19]. The values of FWHM can be further utilized to calculate the average grain sizes through the Scherrer equation [20], by which both sizes for the DAST single crystals grown with and without the OA control were estimated to be similarly about 90 nm. It should be noted that the peak intensities of the DAST grown under the control of the OA at (002), (004), (006), and (008) face are 3.45, 1.76, 2.03, and 2.28 times greater than those of the DAST grown without the OA control, respectively (Figure 4). This suggests that the existence of OA during the growth progress improves the crystallinity of the DAST single crystals.
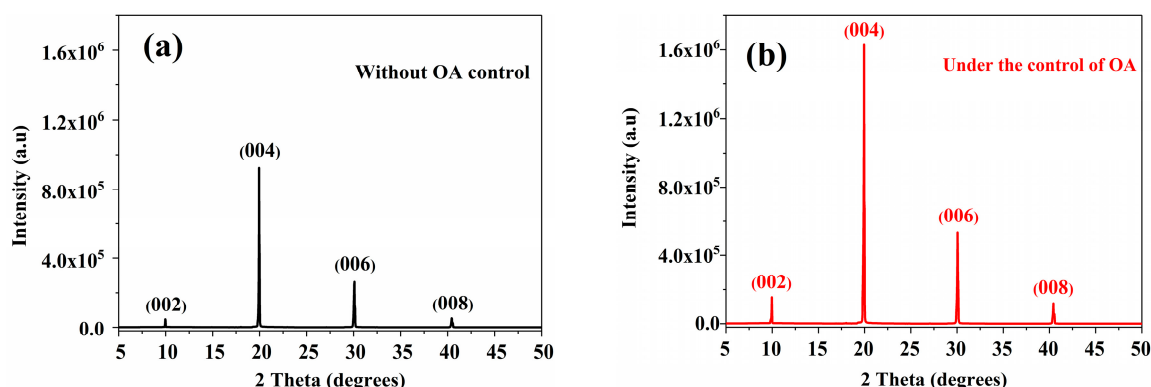
Figure 4. X-ray diffraction patterns observed for the DAST single crystals grown (**a**) without the OA control; (**b**) under the control of the OA.

A femtosecond pulse laser was launched into the DAST crystals grown with and without the OA control, and the resulting SHG signals were collected using a microscope and detected by a spectrometer (SP 2500i, Teledyne Acton Optics, Acton, MA, USA). The related results in Figure 5 show

that strong SHG signals have been measured from both the DAST crystals, and importantly, the optical nonlinearity of the DAST crystal grown under the control of the OA is similar with that conventionally grown without the OA, consistent with the crystallography observation from the XRD measurements (Figure 4).
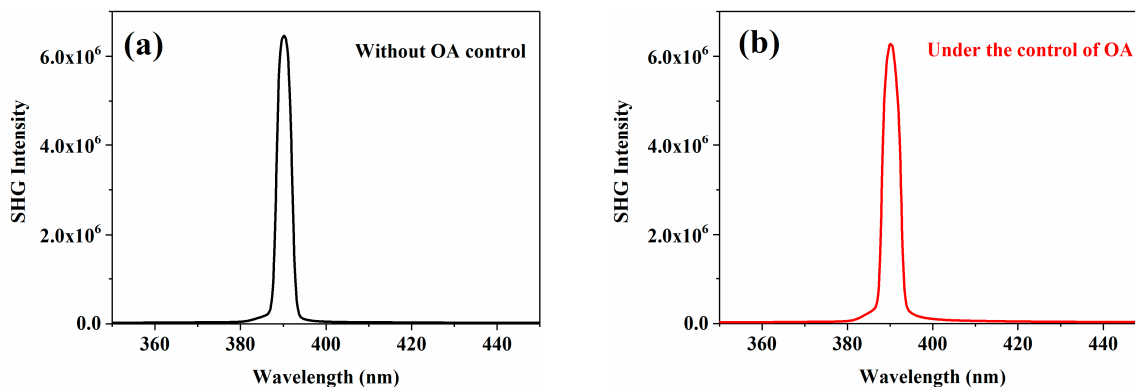
Figure 5. SHG spectra excited by a femtosecond pulse laser for the DAST single crystals grown (**a**) without the OA control; (**b**) under the control of the OA.

The crystals were further characterized by UV-vis spectroscopy to investigate the influences of the OA additive on the optical properties of the as-grown DAST crystals. The absorption spectra of the DAST grown with and without the OA control are depicted in Figure 6. The absorption spectrum of the DAST crystal grown without the OA control by the slow-cooling method as in this work exhibits some subtle differences from those previously grown by the slow solvent evaporation method [19]. This is not entirely a surprise since different growth methods lead to different absorption peaks of the products, due to different preparations, interfaces, surface conditions, and imperfections. In our work, the DAST single crystals were grown with and without the OA control by the slow-cooling method under otherwise the same conditions. Further inspection indicates that the absorption spectrum of the DAST crystal grown without the OA control changes more gently with the wavelength (Figure 6). In contrast, the DAST grown under the control of the OA exhibits a stronger and more clearly discernable absorption edge (Figure 6). It should be noted that compared with the DAST single crystals grown without the OA control, less absorption peaks were measured from the DAST single crystals grown under the control of the OA (Figure 6), further indicating higher crystallinity for the latter case, as suggested by the XRD results (Figure 4).
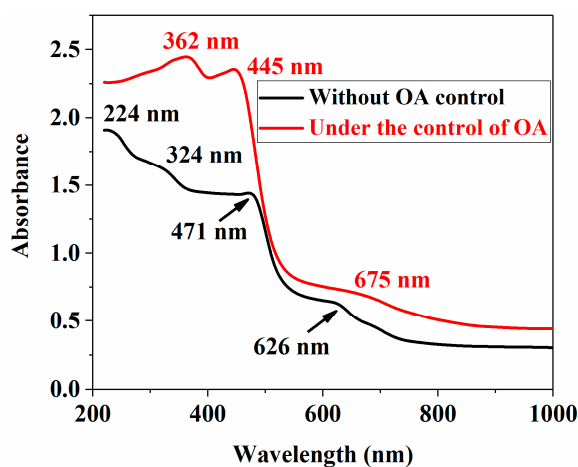
Figure 6. The UV-vis absorbance spectra of the DAST single crystals grown with and without the OA control.

According to the UV-vis measurement results (Figure 6), the optical absorption coefficient can be further determined from the transmittance data (Figure 7a), using the following relation [21]:

$$\alpha = 2.303 \times \log(1/T)/t \tag{1}$$

where T is the transmittance and t is the thickness of the crystal. The optical band gaps of both the DAST single crystals were also estimated by the Tauc plot [22,23]:

$$(\alpha h v)^2 = A(h v - E_g) \tag{2}$$

where α is the optical absorption coefficient, $h v$ is the photon energy associated with the incident wavelength, A is a constant, and E_g is the optical band gap. Figure 7b shows the plot of $(\alpha h v)^2$ versus $h v$ for both the DAST single crystals. The value of the Tauc optical band gap was estimated to be 2.33 eV for the DAST crystal grown without the OA control (Figure 7b), agreeing well with those previously reported [24,25]. It should be noted that a higher E_g of 2.43 eV was measured from the DAST crystal grown under the control of the OA (Figure 7b). According to the results reported by Mondal et al. [26], the reduction in the slope of the linear portion of the Tauc plot suggests the introduction of defect states within the band gap, due to the coupling of an impurity band into the conduction band, thus reducing the optical band gap. According to the UV-vis measurement results, the defect density can be further semi-quantitatively investigated by a near edge absorptivity ratio (NEAR) [27]:

$$\text{NEAR} = 1.02 \left[\frac{(\alpha h v)^2 \big| h v = E_g}{(\alpha h v)^2 \big| h v = 1.02 E_g} \right]^{1/2} \tag{3}$$

The smaller NEAR value suggests lower defect density in a material [27]. Further calculations about the related NEAR value in our work reveal that the NEAR of the crystal grown without the OA control was calculated to be 0.92, while a lower NEAR of 0.86 was estimated from the crystal grown under the control of the OA. This implies that the addition of the OA into the DAST solutions leads to the growth of the DAST single crystals with a wider band gap compared with those grown without the OA control, attributed to higher crystallinity and lower defect density for the former DAST crystals, as indicated by the XRD (Figure 4). The systematic results (Figures 2–7) presented in this work disclose that the DAST single crystals grown under the control of the OA exhibit larger sizes and higher crystallinity and crystal quality, thus suggesting great potential applications of the as-grown DAST crystals in nonlinear optics.
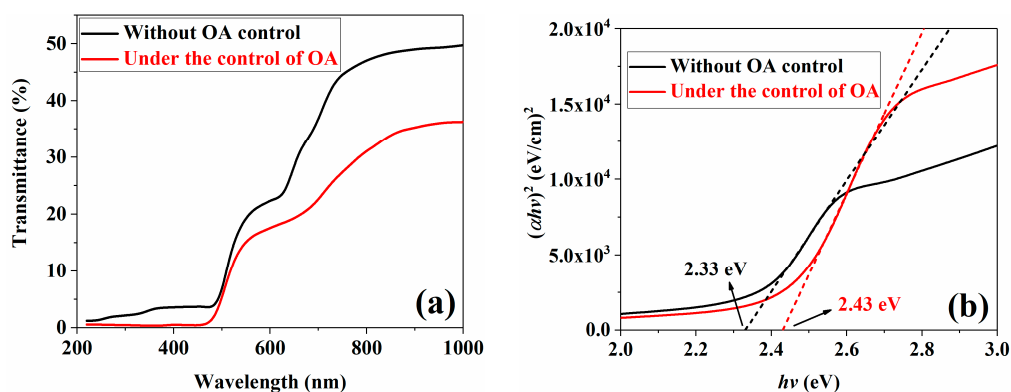
Figure 7. (**a**) UV-vis transmittance spectra of the DAST single crystals grown with and without the OA control; (**b**) Plots of $(\alpha h v)^2$ function against $h v$ with evaluation of the band gaps for various DAST single crystals.

4. Conclusions

In summary, the DAST single crystals grown with and without the control of oleic acid by the slow-cooling method were systematically investigated. Characterizations reveal that the addition of oleic acid during the growth does not induce any chemical or structural change. Unexpectedly, the DAST single crystals grown under the control of the oleic acid exhibit significantly improved crystallinity, and higher optical properties with wider optical band gap and lower defect density, as compared to those DAST crystals grown without the oleic acid control. The valuable and systematic information presented in this work, including the related chemical structures, optical properties, and XRD and UV-vis spectral features, will be helpful for better understanding the growth and applications of DAST single crystals. Future investigations in the pursuit of larger and better DAST crystals could benefit from the findings from this approach of combining appropriate growth methods with additives. The obtained results from the as-grown high quality DAST crystals are rather encouraging for the development of the nonlinear optics and optoelectronic devices.

Author Contributions: Conceptualization, H.Z. and L.H.; methodology, X.C.; validation, Y.J.; investigation, H.Z.; resources, J.S. and X.L.; writing—original draft preparation, X.W.; writing—review and editing, X.X. and J.X.; visualization, X.W.; supervision, X.X.; project administration, T.F., M.Z. and Y.G.

Conflicts of Interest: The authors declare no conflict of interest.

References

1. Marder, S.R.; Perry, J.W.; Schaefer, W.P. Synthesis of organic salts with large second-order optical nonlinearities. *Science* **1989**, *245*, 626–628. [CrossRef] [PubMed]

2. Han, P.Y.; Tani, M.; Pan, F.; Zhang, X.C. Use of the organic crystal DAST for terahertz beam applications. *Opt. Lett.* **2000**, *25*, 675–677. [CrossRef] [PubMed]

3. Yang, Z.; Aravazhi, S.; Schneider, A.; Seiler, P.; Jazbinsek, M.; Günter, P. Synthesis and crystal growth of stilbazolium derivatives for second-order nonlinear optics. *Adv. Funct. Mater.* **2005**, *15*, 1072–1076. [CrossRef]

4. Zhuang, S.J.; Teng, B.; Cao, L.F.; Zhong, D.G.; Feng, K.; Shi, Y.X.; Li, Y.N.; Guo, Q.J.; Yang, M.S. The synthesis and purification of 4-dimethylamino-N-methyl-4-stilbazolium tosylate. *Adv. Mater. Res.* **2013**, *709*, 36–39. [CrossRef]

5. Xu, X.D.; Sun, Z.Q.; Fan, K.; Jiang, Y.D.; Huang, R.; Wen, Y.J.; He, Q.; Ao, T.H. Conversion of 4-N,N-dimethylamino-4′-N′-methyl-stilbazolium tosylate (DAST) from a simple optical material to a versatile optoelectronic material. *Sci. Rep.* **2015**, *5*, 12269. [CrossRef]

6. Fan, K.; Xu, X.D.; Gu, Y.; Dai, Z.L.; Cheng, X.M.; Zhou, J.; Jiang, Y.D.; Fan, T.; Xu, J. Organic DAST single crystal meta-cavity resonances at terahertz frequencies. *ACS Photonics* **2019**, *6*, 1674–1680. [CrossRef]

7. Pan, F.; Knöpfle, G.; Bosshard, C.; Follonier, S.; Spreiter, R.; Wong, M.S.; Günter, P. Electro-optic properties of the organic salt 4-N,N-dimethylamino-4′-N′-methyl-stilbazolium tosylate. *Appl. Phys. Lett.* **1996**, *69*, 13–15. [CrossRef]

8. Meier, U.; Bösch, M.; Bosshard, C.; Pan, F.; Günter, P. Parametric interactions in the organic salt 4-N,N-dimethylamino-4′-N′-methyl-stilbazolium tosylate at telecommunication wavelengths. *J. Appl. Phys.* **1998**, *83*, 3486–3489. [CrossRef]

9. Haja Hameed, A.S.; Yu, W.C.; Chen, Z.B.; Tai, C.Y.; Lan, C.W. An investigation on the growth and characterization of DAST crystals grown by two zone growth technique. *J. Cryst. Growth* **2005**, *282*, 117–124. [CrossRef]

10. Hosokawa, Y.; Adachi, H.; Yoshimura, M.; Mori, Y.; Sasaki, T.; Masuhara, H. Femtosecond laser-induced crystallization of 4-(dimethylamino)-N-methyl-4-stilbazolium tosylate. *Cryst. Growth Des.* **2005**, *5*, 861–863. [CrossRef]

11. Haja Hameed, A.S.; Yu, W.C.; Tai, C.Y.; Lan, C.W. Effect of sodium toluene sulfonate on the nucleation, growth and characterization of DAST single crystals. *J. Cryst. Growth* **2006**, *292*, 510–514. [CrossRef]

12. Bharath, D.; Kalainathan, S.; Anbuselvi, D. Studies on linear and nonlinear optical properties of 4-N,N-dimethylamino-4′-N′-methyl-stilbazolium 2,4,6-trimethylbenzenesulfonate crystal. *J. Mater. Sci. Mater. Electron.* **2018**, *29*, 12813–18123. [CrossRef]

13. Hao, L.; Teng, B.; Cao, L.F.; Zhong, D.G.; Sun, Q.; You, F.; Chang, Q. Effect of toluene-sulfonic acid (PTSA) on the growth and characterization of DAST single crystals. *J. Synth. Cryst.* **2016**, *45*, 540–545.

14. Thomas, T.; Ramaclus, J.V.; Mena, F.P.; Mosquera, E.; Sagayaraj, P.; Michael, E.A. Influence of oleic acid on the nucleation and growth of 4-N,N-dimethylamino-4-N-methyl-stilbazoliumtosylate (DAST) crystals. *CrysTengComm* **2015**, *17*, 1989–1996. [CrossRef]

15. Jagannathan, K.; Kalainathan, S.; Gnanasekaran, T.; Vijayan, N.; Bhagavannarayana, G. Growth and characterization of the NLO crystal 4-dimethylamino-N-methyl-4-stilbazolium tosylate (DAST). *Cryst. Growth Des.* **2007**, *7*, 859–863. [CrossRef]

16. Jagannathan, K.; Kalainathan, S. Growth and characterization of 4-dimethylamino-N-methyl 4-stilbazolium tosylate (DAST) single crystals grown by nucleation reduction method. *Mater. Res. Bull.* **2007**, *42*, 1881–1887. [CrossRef]

17. Senthil, K.; Kalainathan, S.; Ruban Kumar, A. Effect of additives on the large-size growth of 4-N, N-dimethylamino-4-N-methyl stilbazolium naphthalene-2-sulfonate (DSNS) single crystal: An efficient stilbazolium derivative NLO crystal with potential terahertz wave properties. *CrystEngComm* **2014**, *16*, 9847–9856. [CrossRef]

18. Vijayakumar, T.; Hubert Joe, I.; Reghunadhan Nair, C.P.; Jazbinsek, M.; Jayakumar, V.S. Electron-phonon coupling and vibrational modes contributing to linear electro-optic effect of the efficient NLO chromophore 4-(N,N-dimethylamino)-N-methyl-4′-toluene sulfonate (DAST) from their vibrational spectra. *J. Raman Spectrosc.* **2009**, *40*, 52–63. [CrossRef]

19. Manivannan, M.; Martin Britto Dhas, S.A.; Jose, M. Photoacoustic and dielectric spectroscopic studies of 4-dimethylamino-n-methyl-4-stilbazolium tosylate single crystal: An efficient terahertz emitter. *J. Cryst. Growth* **2016**, *455*, 161–167. [CrossRef]

20. He, K.; Chen, N.F.; Wang, C.J.; Wei, L.S.; Chen, J.K. Method for determining crystal grain size by X-ray diffraction. *Cryst. Res. Technol.* **2018**, *53*, 1700157. [CrossRef]

21. Bhandari, S.; Sinha, N.; Ray, G.; Kumar, B. Enhanced optical, dielectric and piezoelectric behavior in dye doped zinc tris-thiourea sulphate (ZTS) single crystals. *Chem. Phys. Lett.* **2014**, *591*, 10–15. [CrossRef]

22. Tauc, J.; Menth, A. States in the gap. *J. Non-Cryst. Solids* **1972**, *8–10*, 569–585. [CrossRef]

23. Mahendra, K.; Kumar, H.K.T.; Udayashankar, N.K. Enhanced structural, optical, thermal, mechanical and electrical properties by a noval approach (nanoparticle doping) on ferroelectric triglycine sulphate single crystal. *Appl. Phys. A* **2019**, *125*, 228. [CrossRef]

24. Haja Hameed, A.S.; Karthikeyan, C.; Nisha, S.A.; Louis, G.; Ravi, G. Influence of organic dopants on the optical properties of 4-N,N′-dimethylamino-N′-methyl stilbazolium tosylate crystals. *Optik* **2016**, *127*, 4011–4018. [CrossRef]

25. Narsimha Rao, E.; Vaitheeswaran, G. Structure–property correlation studies of potassium 4,4′-Bis(dinitromethyl)-3,3′-azofurazanate: A noncentrosymmetric primary explosive. *J. Phys. Chem. C* **2019**, *123*, 10034–10050. [CrossRef]

26. Mondal, S.; Bhattacharyya, S.R.; Mitra, P. Effect of Al doping on microstructure and optical band gap of ZnO thin film synthesized by successive ion layer adsorption and reaction. *Pramana-J. Phys.* **2013**, *80*, 315–326. [CrossRef]

27. Coulter, J.B.; Birnie, D.P. Assessing Tauc plot slope quantification: ZnO thin films as a model system. *Phys. Status Solidi B* **2018**, *255*, 1700393. [CrossRef]